Supporting Information

Table of Contents

1. Experimental Section

1.1. General

All reagents and starting materials were obtained from commercial suppliers and used without further purification. Anhydrous dichloromethane (DCM) was distilled from CaH_2. Anhydrous toluene and THF were distilled from sodium-benzophenone immediately prior to use. Precursors **1**[1] and **2**[2] were prepared according to literature procedures. The ^{1}H NMR and ^{13}C NMR spectra were recorded in solution of $CDCl_3$/CD_2Cl_2/THF-d_8 on Bruker DPX300/ DPX400/DPX500 NMR spectrometer with tetramethylsilane (TMS) as the internal standard. The following abbreviations were used to explain the multiplicities: s = singlet, d = doublet, t = triplet, m = multiplet. HR-APCI mass spectra (MS) were recorded on a Bruker amazon instrument. EI mass spectra were recorded on Agilent 5975C DIP/MS mass spectrometer. Steady-state UV-vis absorption were recorded on a Shimadzu UV-1700 and UV-3600 spectrometer. The electrochemical measurements were carried out in anhydrous DCM with 0.1 M tetrabutylammonium hexafluorophosphate (n-Bu_4NPF_6) as the supporting electrolyte at room temperature under the protection of nitrogen. A gold stick was used as working electrode, platinum wire was used as counting electrode, and Ag/AgCl (3M KCl solution) as reference electrode. The potential was externally calibrated against the ferrocene/ferrocenium couple. The single crystal was measured at low temperature (T = 100K) on a four circles goniometer Kappa geometry Bruker AXS D8 Venture equipped with a Photon 100 CMOS active pixel sensor detector using a Copper monochromatized (λ = 1.54178 Å) X-ray radiation.

Continuous wave X-band ESR spectra were obtained with a JEOL (FA200) spectrometer using a variable temperature liquid nitrogen cryostat. The VT ESR data of **MC4-S** and **CPTP-M** in the frozen solutions were fitted by Bleaney-Bowers equation (1),

$$IT = \frac{C}{k_B[3+exp(-2J/k_BT)]} \quad (1)$$

where C is a constant and -2J is correlated to the excitation energy from the ground state to the first excited state.

1.2. Synthetic procedures and characterization data

Synthesis of macrocycle 3 by Suzuki coupling reaction.

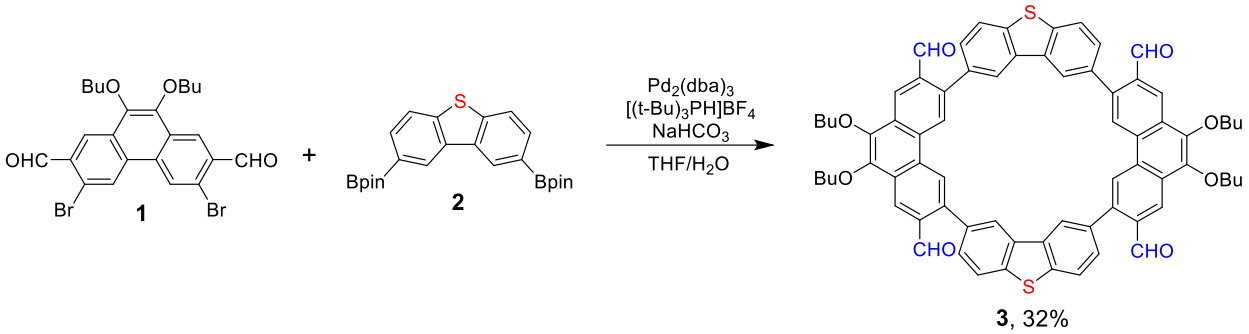

A mixture of **1** (200 mg, 0.37 mmol), **2** (163 mg, 0.37 mmol), $NaHCO_3$ (1.5 g, 17.86 mmol), THF (2500 mL) and H_2O (15 mL), was carefully degassed before $Pd_2(dba)_3$ (34 mg, 0.037 mmol), and $[(t\text{-}Bu)_3PH]BF_4$ (43 mg, 0.149 mmol) were added. The mixture was stirred and heated at 80 °C under nitrogen atmosphere for 2 days. The organic solvent was removed under reduced pressure, and then H_2O and DCM were added. The organic layer was separated, dried over anhydrous sodium sulfate, and evaporated to dryness. The residue was first purified by a short column chromatography (silica gel, DCM/Hexane = 2:1) to remove catalysts, and then further purified on by preparative GPC using $CHCl_3$ at a rate of 14 mL/min. Yellow solid macrocycle **3** was obtained in 32% yield (75 mg). ^{1}H NMR (400 MHz, $CDCl_3$, δ ppm): 10.20 (s, 4H), 9.01 (s, 4H), 8.85 (s, 4H), 8.59-8.58 (d, 4H, J = 1.4 Hz), 7.99-7.97 (d, 4H, J = 8.1 Hz), 7.48-7.46 (m, 4H), 4.39-4.30 (m, 8H), 2.01-1.94 (m, 8H), 1.71-1.61 (m, 8H), 1.08-1.05 (t, 12H, J = 7.4 Hz). ^{13}C NMR (100 MHz, $CDCl_3$, δ ppm): 191.82, 144.08, 141.45, 140.00, 135.91, 135.10, 133.24, 130.84, 130.61, 130.15, 126.17, 124.24, 122.47, 122.27, 73.85, 32.48, 19.43, 14.00. HRMS (APCI, m/z): $[(M+H)^+]$ calcd for $C_{72}H_{61}O_8S_2$, 1117.3802; found, 117.3791.

Synthesis of compound MC4-S.

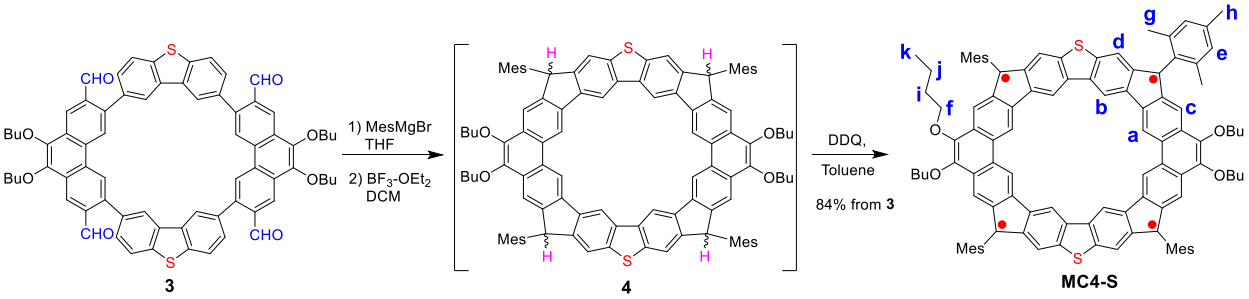

Under nitrogen atmosphere, 2-mesitylmagnesium bromide (1 M solution in THF, 0.5 mL) was added to the solution of compound **3** (40 mg, 0.036 mmol) in dry THF (20 mL) and the solution was stirred at room temperature overnight. The reaction solution was quenched by water and extracted by DCM. The organic layer was dried over Na_2SO_4 and the solvent was removed under reduced pressure. The crude product was then dissolved in 20 mL of dry DCM under nitrogen atmosphere and 0.05 mL of $BF_3{\cdot}OEt_2$ was added. The mixture was stirred for 3 hours and the solvent was removed under reduced pressure. The residue was purified by flash column chromatography (silica gel, DCM/Hexane = 1:1) to give the cyclic product (**4**), which was used directly for the next step. It was dissolved in 10 mL of dry toluene under nitrogen atmosphere, and then DDQ (16 mg, 0.072 mmol) was added and the mixture was stirred for 6 hours at room temperature. The solvent was removed under reduced pressure and the residue was purified by flash column chromatography (silica gel, DCM/Hexane = 1:1). Black solid compound **MC4-S** (46 mg) was obtained in 84% yield over three steps from **3**. ^{1}H NMR (500 MHz, CD_2Cl_2, 183K, δ ppm): 15.49 (s, 1H), 14.92 (s, 1H), 6.53 (s, 2H), 4.63 (s, 1H), 4.08 (s, 1H), 3.17 (s, 2H), 1.98 (s, 3H), 1.87 (s, 6H), 1.04 (s, 2H), 0.78 (s, 2H), 0.51 (s, 2H). HRMS (APCI, m/z): [$(M+H)^+$] calcd for $C_{108}H_{97}O_4S_4^{4\bullet}$, 1521.6823; found, 1521.6820.

Synthesis of the dication MC4-S^{2+}

NO•SbF_6 (1.8 mg, 0.0066 mmol) dissolved in dry acetonitrile (50 μL) was added into the solution of **MC4-S** (5.0 mg, 0.0033 mmol) in dry DCM (2 mL). The oxidized compound was formed in 3 minutes, and the solvent was removed under vacuum to give the dication **MC4-S^{2+}** without further purification. ^{1}H NMR (500 MHz, CD_2Cl_2, δ ppm, under protection of nitrogen): 13.73 (s, 1H), 13.17 (s, 1H), 8.09 (s, 2H), 5.84 (t, 2H, J = 6.0 Hz), 3.09 (s, 3H), 2.85-2.79 (m, 2H), 2.41-2.34 (m, 2H), 1.93-1.91 (m, 2H). Due to its instability under ambient condition, its mass spectrum was not collected.

2. Additional spectra

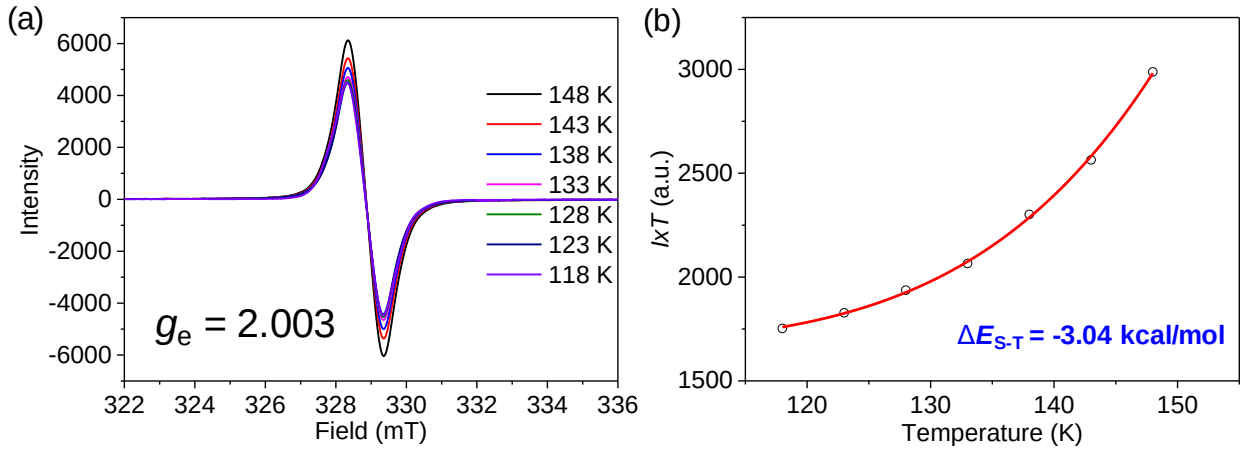

Figure S1. (a) VT ESR spectra of **CPTP-M** in frozen DCM solution. (b) *I*×*T*-*T* plot of **CPTP-M** in frozen DCM and the red line is the fitted curve.

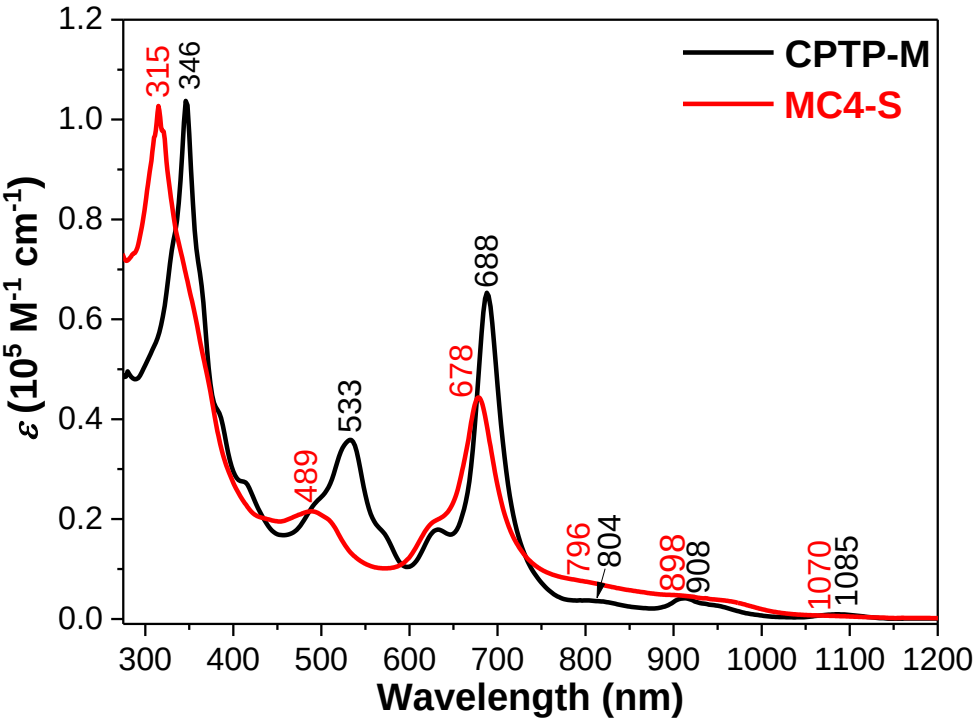

Figure S2. A comparison of the UV-Vis-NIR absorption spectrum of **MC4-S** with that of **CPTP-M** in DCM.

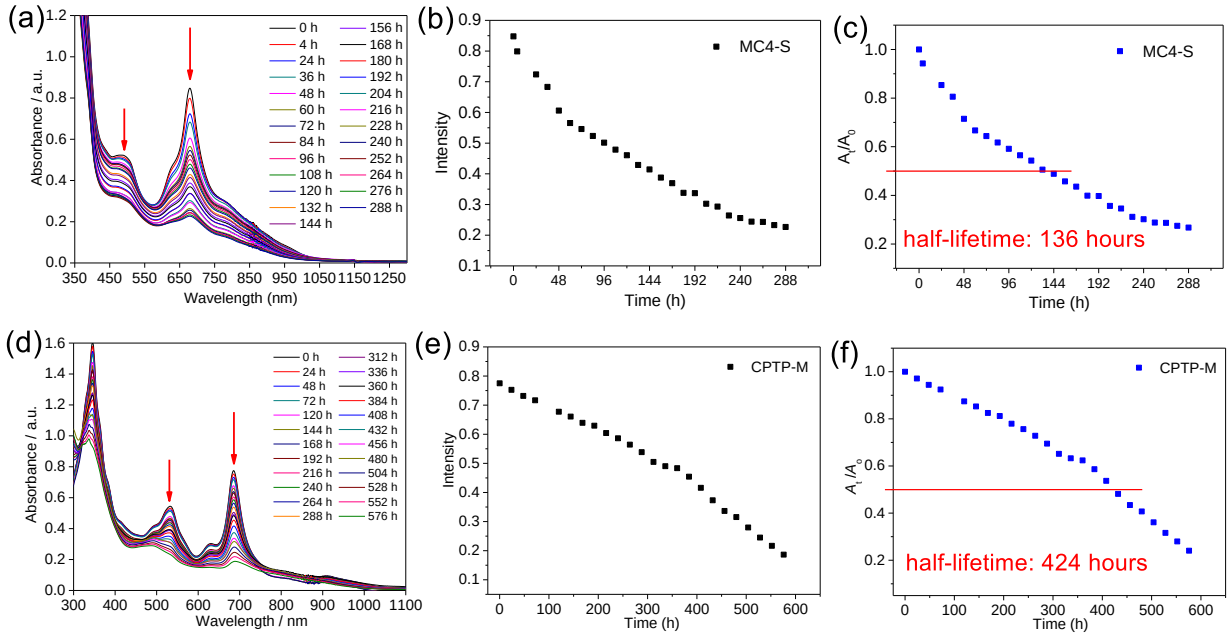

Figure S3. Change of the absorption spectrum of **MC4-S** (a) and **CPTP-M** (d) in DCM with time under ambient air and light conditions, and plots of the absorbance of **MC4-S** (b, c) at 678 nm and **CPTP-M** (e, f) at 684 nm with time. The half-life time ($t_{1/2}$) is defined as the time when the absorbance decreased to that half of the original absorbance at the selected wavelength.

3. Theoretical calculations

The geometry optimization was performed with the Gaussian09 program suite,[3] and all calculations were carried out using the density functional theory (DFT) method with Becke's threeparameter hybrid exchange functionals and the Lee-Yang-Parr correlation functional (B3LYP) employing the 6-31G(d,p) basis set for all atoms.[4] Time-dependent DFT (TD-DFT) calculations have been performed at the B3LYP/6-31G(d,p) level of theory with CPCM model. The radical character of the electronic ground state and transition energies to higher states of **MC4-S** were calculated using the spin unrestricted RAS-SF/6-31G(d) method based on the geometry optimized at the UB3LYP/6-31G(d,p) level of theory.[5] The radical character of the open-shell singlet ground state singlet was estimated by the number of unpaired electrons (N_U) according to equation 2, where $\{n_i\}$ are the natural occupation numbers from the one-particle density matrix.

$$N_U = \sum_i \left(1 - abs(1 - n_i)\right) \qquad (2)$$

NICS values were calculated (UB3LYP/6-31G(d,p)) using the standard GIAO procedure (NMR pop=NCSall).[6] AICD plot (UB3LYP/6-31G(d,p)) was calculated by using the method developed by Herges.[7] The iso-chemical shielding surface (ICSS)[8] calculations were carried out to analyze two-dimensional nucleus induced chemical shifts (2D-NICS) depending on various planes.

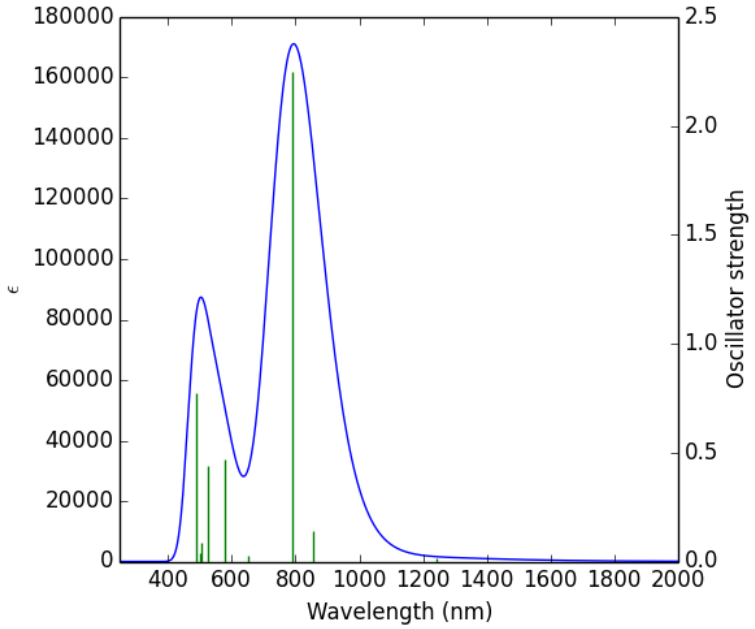

Figure S4. TD DFT simulated spectrum of **MC4-S** in DCM.

Table S1. Selected TD-DFT (RB3LYP/6-31G*) calculated energies, oscillator strength and compositions of major electronic transitions of **MC4-S**.

Wavelength (nm)	Osc.Strength (f)	Major contributions
1971	0.0	HOMO->LUMO (100%)
1242	0.0161	H-1->LUMO (31%), HOMO->L+1 (68%)
855	0.1413	H-2->LUMO (86%), H-1->LUMO (10%) , H-5->L+1 (3%)
820	0.0	H-1->L+1 (91%), H-2->L+1 (7%)
791	2.25	H-2->LUMO (12%), H-1->LUMO (60%), HOMO->L+1 (31%)
715	0.0	H-5->LUMO (17%), H-2->L+1 (76%), H-1->L+1 (5%)
709	0.0	H-3->LUMO (97%)
650	0.0291	H-4->LUMO (66%), H-3->L+1 (32%)
587	0.0	H-5->LUMO (80%), H-2->L+1 (16%)
579	0.4677	H-4->LUMO (30%), H-3->L+1 (66%), HOMO->L+4 (2%)

560	0.0	H-4->L+1 (93%)
526	0.4389	H-8->LUMO (21%), H-5->L+1 (73%)
515	0.0	HOMO->L+2 (96%)
505	0.0	H-7->L+1 (11%), H-6->LUMO (87%)
505	0.0837	H-7->LUMO (86%), H-6->L+1 (12%)
504	0.0	H-9->LUMO (89%), H-8->L+1 (9%)
501	0.0375	H-8->LUMO (48%), H-5->L+1 (11%), HOMO->L+3 (33%), H-9->L+1 (5%)
487	0.7724	H-8->LUMO (20%), H-5->L+1 (10%), HOMO->L+3 (61%), H-14->LUMO (2%), H-9->L+1 (3%)
475	0.0	H-12->L+1 (10%), H-10->LUMO (89%)
474	0.0	H-13->L+1 (10%), H-11->LUMO (90%)

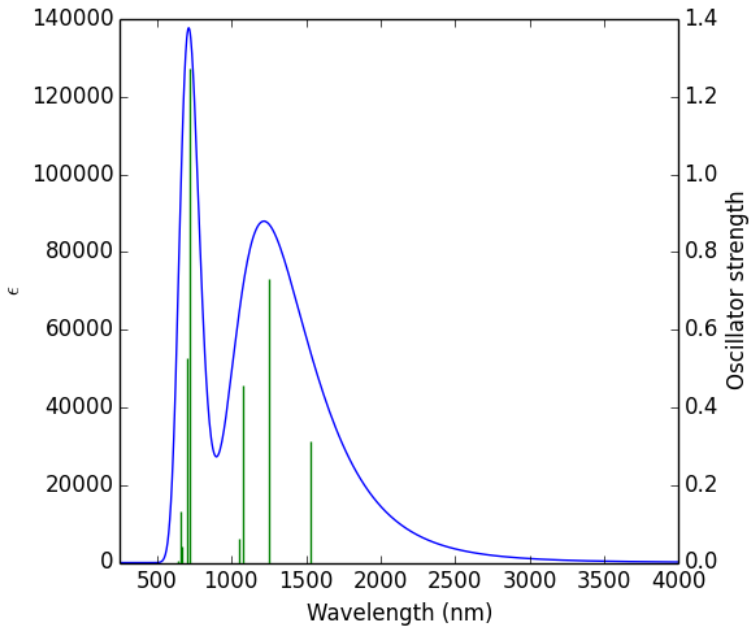

Figure S5. TD DFT simulated spectrum of **MC4-S^{2+}** in DCM.

Table S2. Selected TD-DFT (RB3LYP/6-31G*) calculated energies, oscillator strength and compositions of major electronic transitions of **MC4-S^{2+}**.

Wavelength (nm)	Osc.Strength (f)	Major contributions
1530	0.314	H-1->LUMO (17%), HOMO->LUMO (83%)

1252	0.7302	HOMO->L+1 (91%), H-3->LUMO (9%), H-1->L+1 (3%)
1080	0.4561	H-1->LUMO (78%), HOMO->LUMO (15%), H-3->L+1 (8%)
1051	0.0629	H-1->L+1 (93%), H-3->LUMO (4%)
989	0.0	H-2->LUMO (68%), HOMO->L+2 (24%), H-1->L+2 (7%)
854	0.0	H-2->LUMO (20%), HOMO->L+2 (70%), H-4->L+1 (6%)
847	0.0	H-2->L+1 (92%), H-4->LUMO (5%)
754	0.0	H-4->L+1 (39%), H-2->LUMO (11%), H-1->L+2 (46%)
745	0.0	H-4->LUMO (92%), H-2->L+1 (6%)
721	1.2721	H-3->LUMO (79%), HOMO->L+1 (10%), H-5->LUMO (2%), H-4->L+2 (3%), H-1->L+1 (3%)
703	0.5262	H-3->L+1 (72%), H-2->L+2 (11%), H-8->LUMO (5%), H-1->LUMO (5%), HOMO->LUMO (3%)
674	0.0	H-4->L+1 (48%), H-1->L+2 (41%), H-6->LUMO (3%)
663	0.0	H-7->L+1 (12%), H-6->LUMO (80%), H-4->L+1 (3%), H-1->L+2 (2%)
662	0.0405	H-8->L+1 (13%), H-5->LUMO (78%), H-7->L+2 (2%), H-4->L+2 (4%)
658	0.1336	H-8->LUMO (54%), H-5->L+1 (23%), H-2->L+2 (18%) H-6->L+2 (3%)
650	0.0	H-7->LUMO (79%), H-6->L+1 (15%), H-5->L+2 (3%)
639	0.0	H-12->L+1 (19%), H-11->LUMO (70%) , H-9->L+2 (3%), H-7->L+1 (5%)
638	0.0036	H-9->LUMO (65%), H-9->L+1 (15%), H-11->L+2 (4%), H-10->LUMO (7%), H-10->L+1 (7%)
638	0.0029	H-10->LUMO (66%), H-10->L+1 (15%) , H-12->L+2 (4%), H-9->LUMO (7%), H-9->L+1 (7%)
638	0.0	H-12->LUMO (70%), H-11->L+1 (20%), H-10->L+2 (3%), H-6->L+1 (5%)

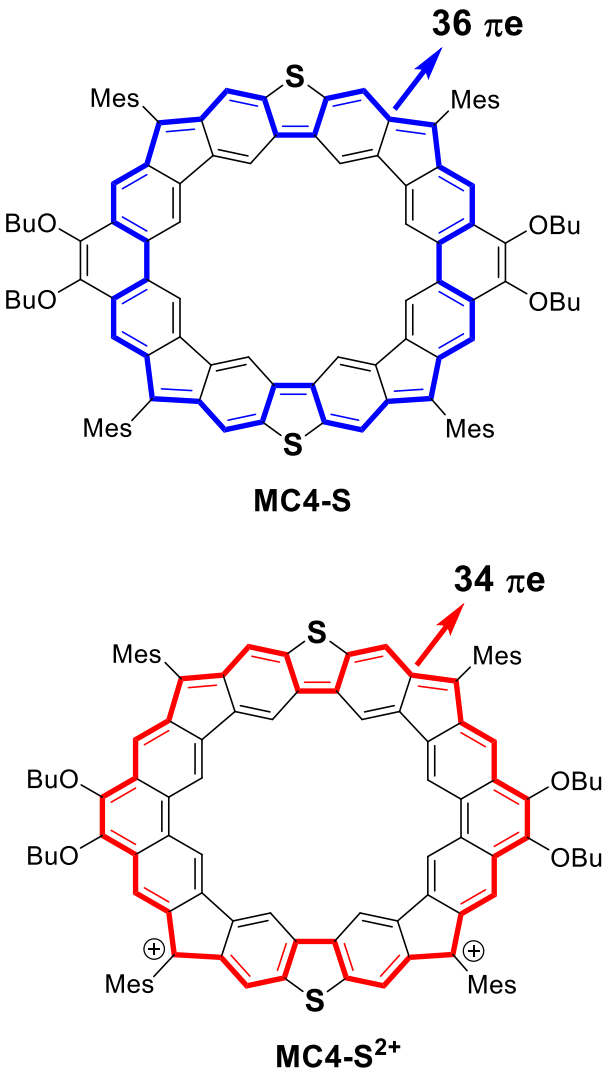

Figure S6. Dominant 36π and 34π conjugation pathways in the backbone of **MC4-S** and **MC4-S^{2+}**.

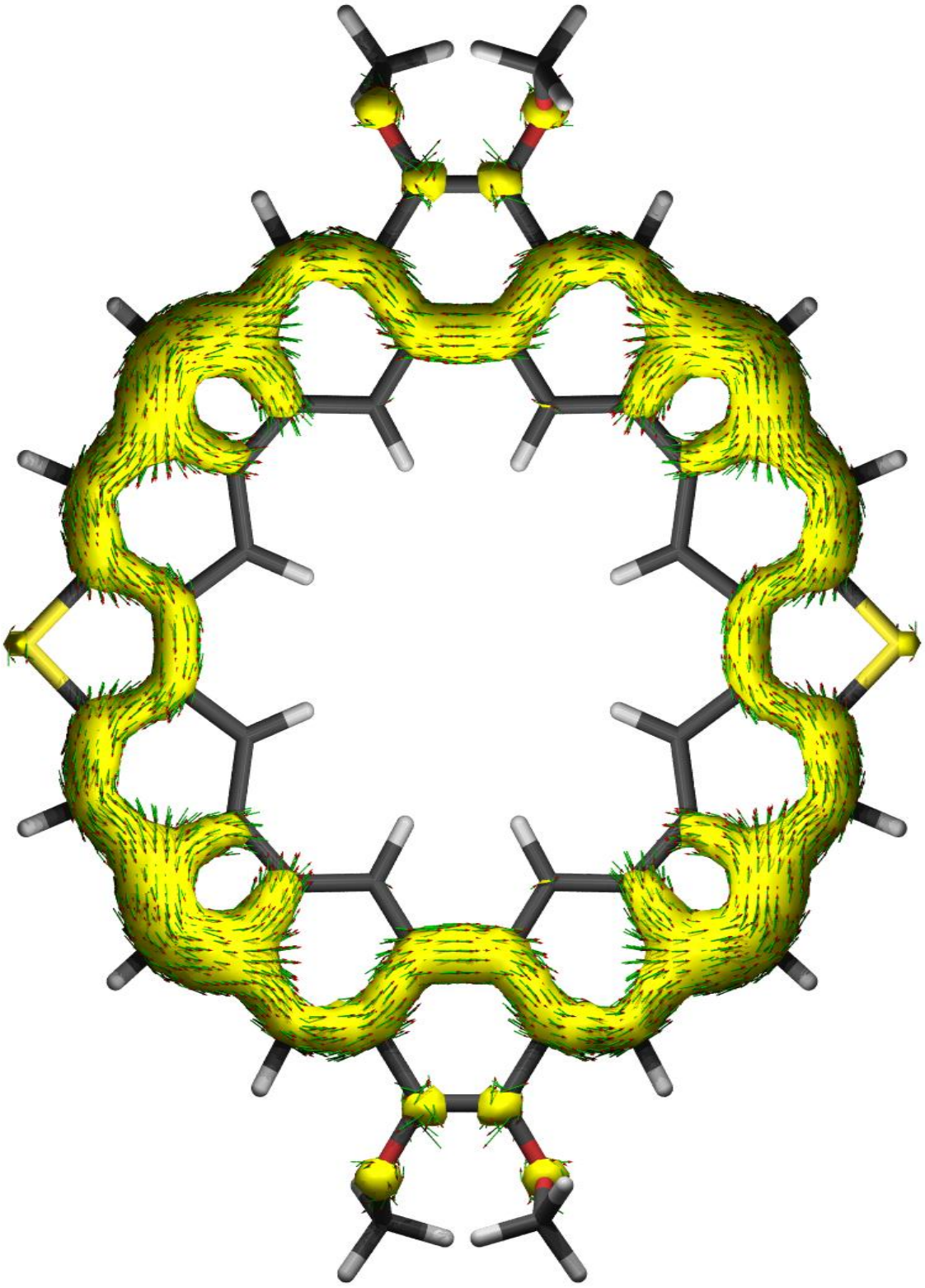

Figure S7. Calculated ACID plot (contribution from π electrons only) of **MC4-S** in the singlet ground state. The magnetic field is perpendicular to the XY plane and points out through the paper.

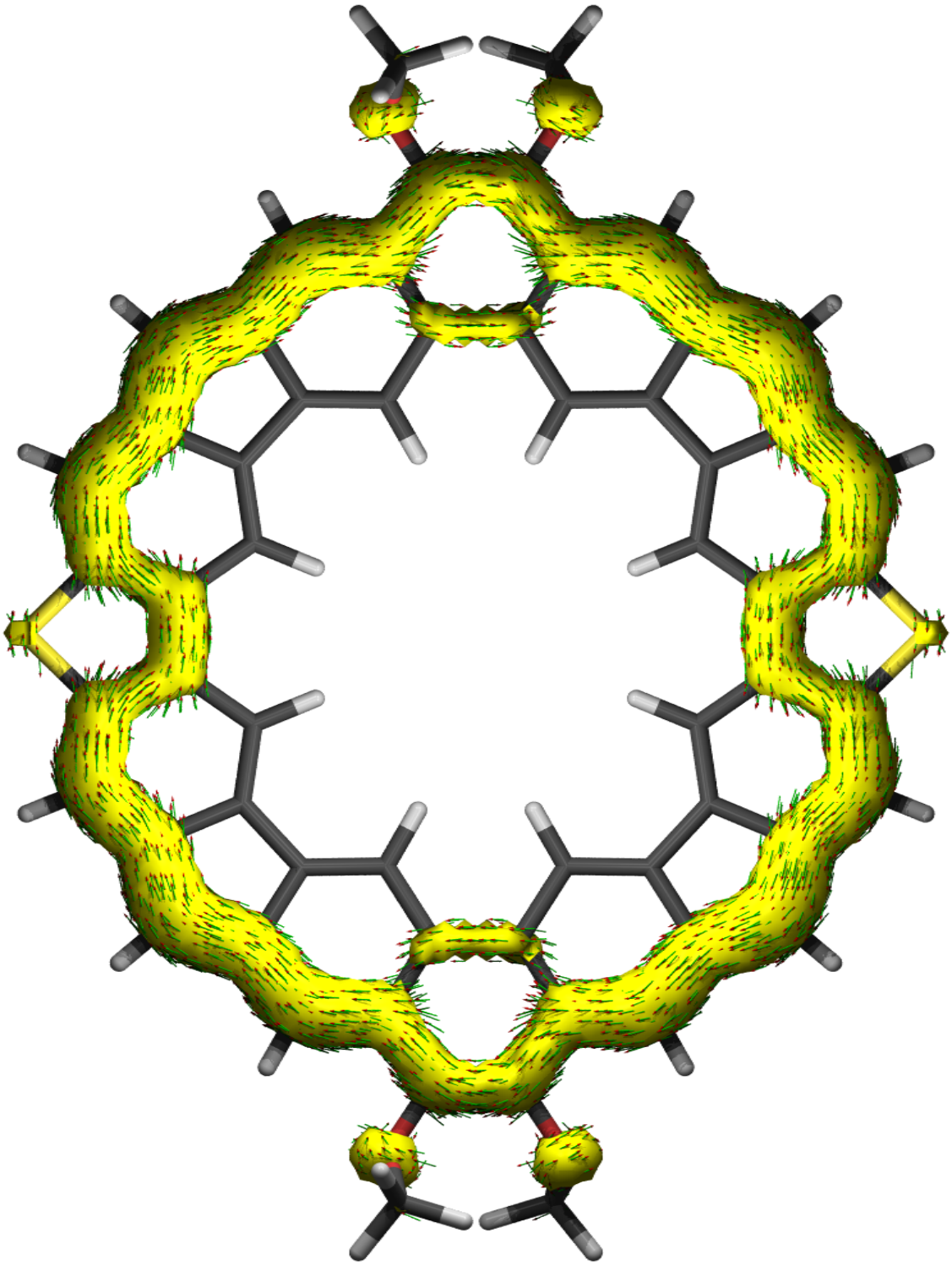

Figure S8. Calculated ACID plot (contribution from π electrons only) of dication **MC4-S^{2+}** in the singlet ground state. The magnetic field is perpendicular to the XY plane and points out through the paper.

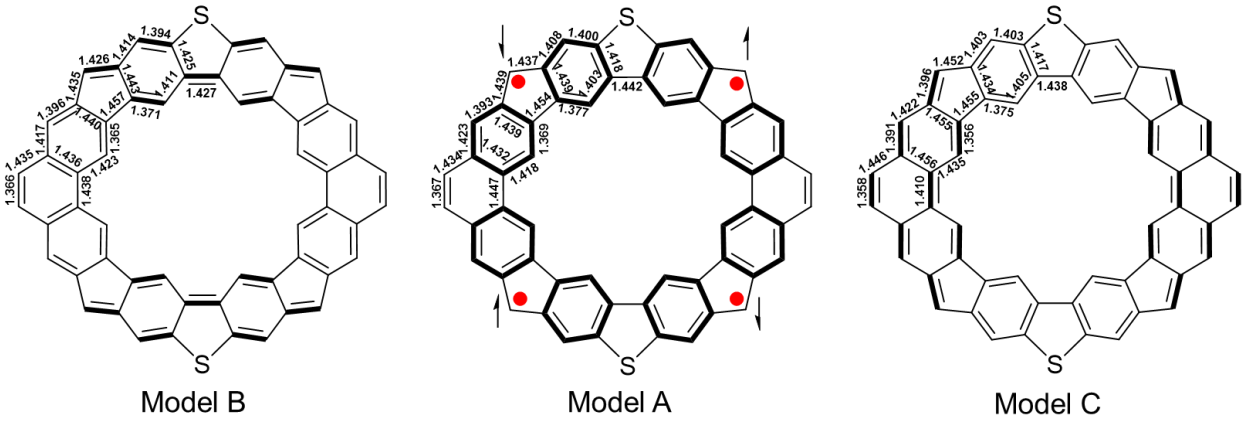

Figure S9. Geometries with different bond localization optimized under UB3LYP/6-31G(d,p) level of theory.

Table S3. Relative electronic energies, diradical characters y_0 and tetraradical characters y_1 calculated from optimized geometries Model A, Model B and Model C with different bond localization under UCAM-B3LYP/6-31G(d,p).

		Model B	**Model A**	**Model C**
UCAM-B3LYP/6-31G(d,p)	Relative Energy (kJ/mol)	0	1.1	33.0
	y_0	0.88399	0.93995	0.35994
	y_1	0.26491	0.31193	0.32635
ULC-BLYP/6-31G(d)	Relative Energy (kJ/mol)	0	1.1	34.3
	y_0	0.92011	0.96597	0.46078
	y_1	0.39877	0.44693	0.44400

The substituents-free structure of MC4-S, namely Model B was optimized under UB3LYP/6-31G(d,p) to further evaluate the bond localization. As revealed from Figure S9, the bond

alternation is almost the same as shown in single crystal structure. Therefore, the preferred bond localization of MC4-S can be confirmed and the bond length alternation in crystal structure is merely resulted from crystal packing force. To further evaluate the valence tautomerization of MC4-S, Model A, which was an optimized structure of MC4-S at triplet state but still adopt electronic configuration singlet state, was calculated due to the absence of higher D4h symmetry of MC4-S. As shown in figure S9, the structure of Model A resembles a higher symmetry as the bonds at cyclopenta-ring units are almost homogeneous. The energy difference between Model A and B is only 1.1 kJ/mol. Compared to Tobe's structure (10.1002/anie.201410791), this energy gap is much lower. This can be attributed to the extended quinoidal conjugation in MC4-S, resulting smaller singlet-triplet energy gap. Another valence tautomer Model C was also calculated, of which the quinoidal conjugations locate at the phenanthrene units. Such structure optimization can be achieved by using the initial geometry with intended bond localization and optimized with the keyword geom=connectivity. However, the calculated energy of Model C is significantly higher than Model A and B, indicating that bond localization in Model C is not preferred.

Table S4. Calculated chemical shifts of MC4-S and MC4-S^{2+} using GIAO method under UB3LYP/6-31G (d, p) level of theory.

	a	**b**	**c**	**d**	**e**
MC4-S (ppm)	12.41	11.73	7.35	6.42	7.75
MC4-S^{2+} (ppm)	-4.92	-5.25	15.53	14.47	9.29

4. X-ray crystallographic data

The X-ray intensity data of **MC4-S** were measured at low temperature (T=100K), using a four circles goniometer Kappa geometry, Bruker AXS D8 Venture, equipped with a Photon 100 CMOS active pixel sensor detector. Frames were integrated with the Bruker SAINT[9] software package. Data were corrected for absorption effects using the multi-scan method (SADABS).[10] Molecule was solved with the software SHELXT,[11] using a Dual Space method. Refinement of the structure was performed by least squares procedures on weighted F2 values using the SHELXL-version 2014/6[12] included in the WinGx system programs for Windows.[13]

A specimen of $C_{122}H_{112}O_4S_2$ was used for the X-ray crystallographic analysis. The X-ray intensity data were measured (λ = 1.54178 Å). The total exposure time was 6.74 hours. The frames were integrated with the Bruker SAINT software package[7] using a narrow-frame algorithm. The integration of the data using a triclinic unit cell yielded a total of 15810 reflections to a maximum θ angle of 66.58° (0.84 Å resolution), of which 7723 were independent (average redundancy 2.047, completeness = 96.0%, R_{int} = 10.04%, R_{sig} = 13.07%) and 3660 (47.39%) were greater than $2\sigma(F^2)$. The final cell constants of $\underline{a}$ = 8.9363(5) Å, $\underline{b}$ = 15.5536(9) Å, $\underline{c}$ = 17.3731(9) Å, α = 106.709(4)°, β = 97.475(4)°, γ = 95.961(4)°, volume = 2267.6(2) $Å^3$, are based upon the refinement of the XYZ-centroids of 769 reflections above 20 σ(I) with 5.388° < 2θ < 132.6°. Data were corrected for absorption effects using the Multi-Scan method (SADABS). The ratio of minimum to maximum apparent transmission was 0.795.

The structure was solved and refined using the Bruker SHELXTL Software Package, using the space group P -1, with Z = 1 for the formula unit, $C_{122}H_{112}O_4S_2$. The final anisotropic full-matrix least-squares refinement on F^2 with 651 variables converged at R1 = 9.15%, for the observed data and wR2 = 29.01% for all data. The goodness-of-fit was 0.968. The largest peak in the final difference electron density synthesis was 0.585 $e^-/Å^3$ and the largest hole was -0.259 $e^-/Å^3$ with an RMS deviation of 0.074 $e^-/Å^3$. On the basis of the final model, the calculated density was 1.249 g/cm^3 and F(000), 908 e^-.

Crystallographic data for compound **MC4-S** (CCDC no.: 1965057) was deposited in the Cambridge Crystallographic Data Center (CCDC).

Table S5. Crystal data and structure refinement for **MC4-S**.

Identification code	MC4-S

Empirical formula	C122 H112 O4 S2	
Formula weight	1706.23	
Temperature	100(2) K	
Wavelength	1.54178 Å	
Crystal system	Triclinic	
Space group	P-1	
Unit cell dimensions	a = 8.9363(5) Å	a= 106.709(4)°.
	b = 15.5536(9) Å	b= 97.475(4)°.
	c = 17.3731(9) Å	g = 95.961(4)°.
Volume	2267.6(2) Å3	
Z	1	
Density (calculated)	1.249 Mg/m3	
Absorption coefficient	0.979 mm-1	
F(000)	908	
Crystal size	0.126 x 0.050 x 0.040 mm3	
Theta range for data collection	2.694 to 66.583°.	
Index ranges	-10<=h<=9, -18<=k<=17, -20<=l<=20	
Reflections collected	15810	
Independent reflections	7723 [R(int) = 0.1004]	
Completeness to theta = 66.583°	96.0 %	
Absorption correction	Semi-empirical from equivalents	
Max. and min. transmission	0.7528 and 0.5753	
Refinement method	Full-matrix least-squares on F2	
Data / restraints / parameters	7723 / 238 / 651	
Goodness-of-fit on F2	0.968	
Final R indices [I>2sigma(I)]	R1 = 0.0915, wR2 = 0.2296	
R indices (all data)	R1 = 0.1777, wR2 = 0.2901	
Extinction coefficient	n/a	
Largest diff. peak and hole	0.585 and -0.259 e.Å-3	

5. ^{1}H, ^{13}C NMR and HR mass spectra of new compounds

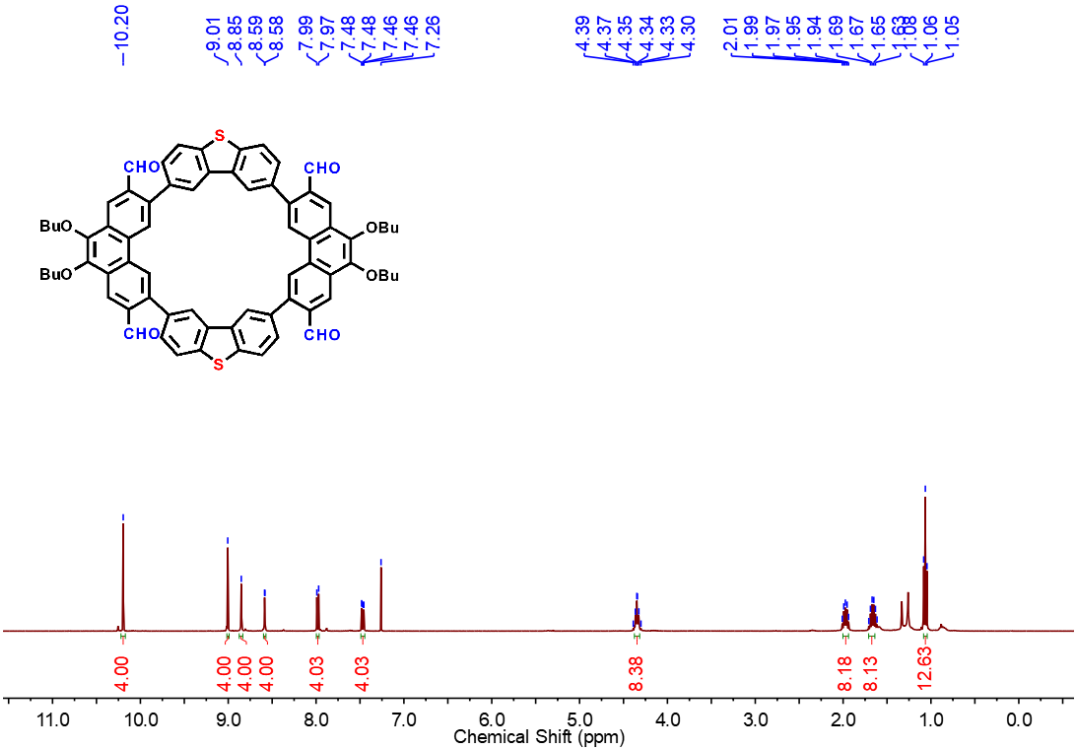

Figure S10. ^{1}H NMR spectrum (500 MHz) of **3** in $CDCl_3$ at 298 K.

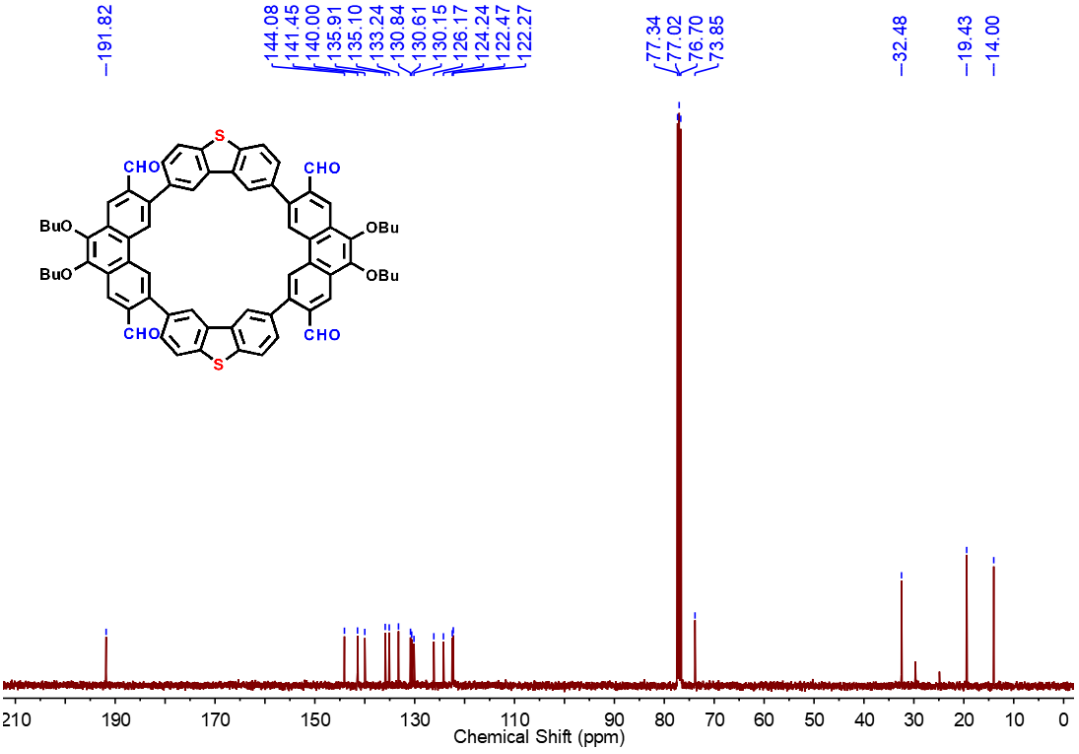

Figure S11. ^{13}C NMR spectrum (100 MHz) of **3** in $CDCl_3$ at 298 K.

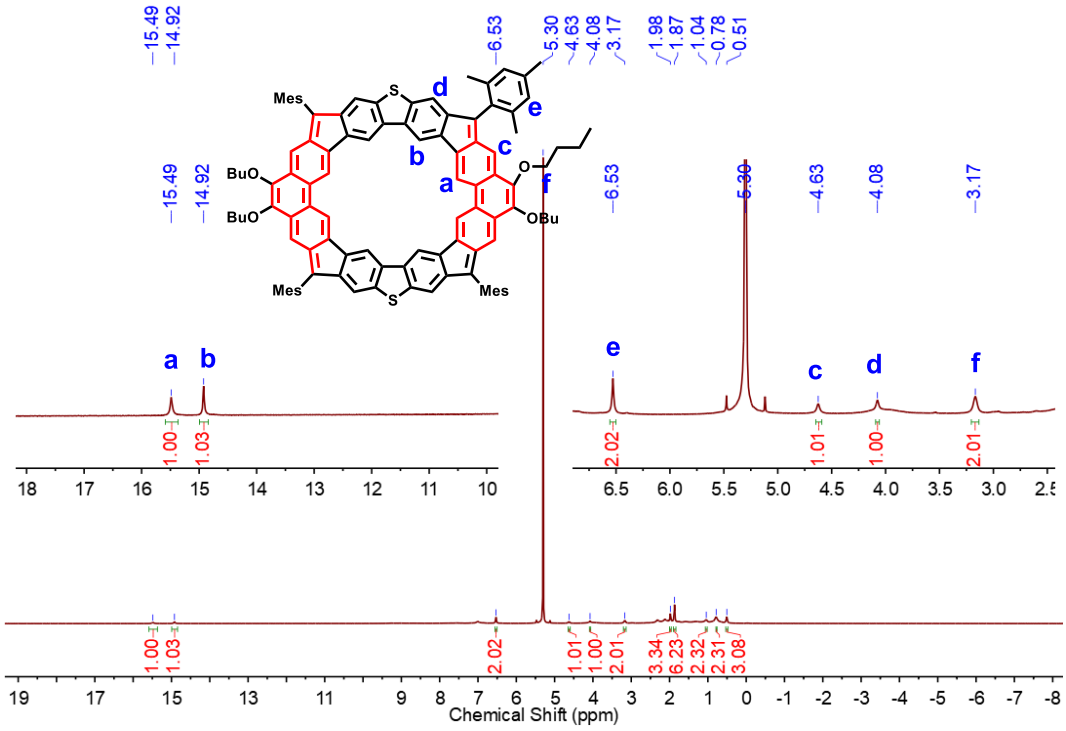

Figure S12. ^{1}H NMR spectra of **MC4-S** in CD_2Cl_2 at 183 K (500 MHz).

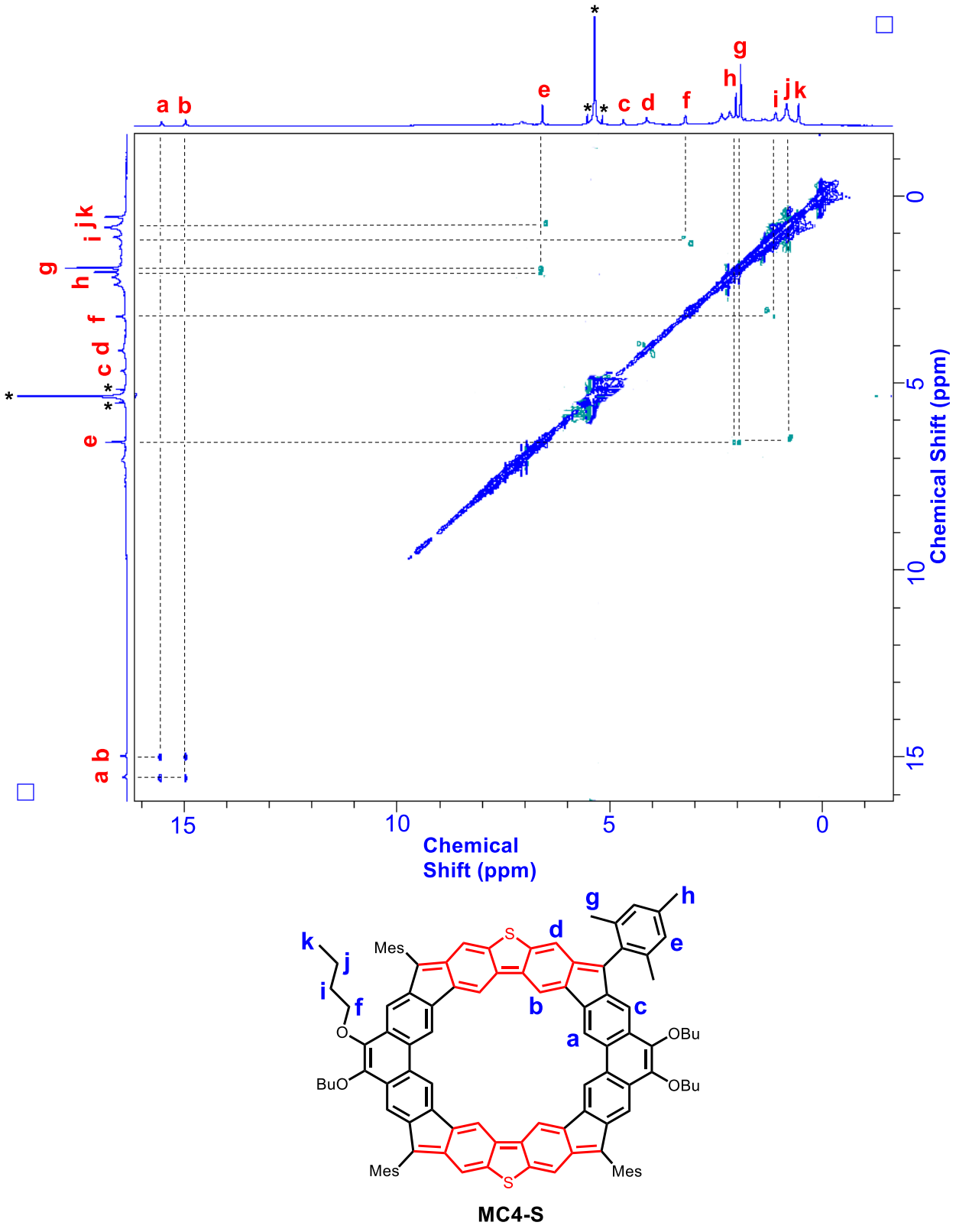

Figure S13. 2D ROESY NMR spectrum of **MC4-S** in CD_2Cl_2 at 183 K (500 MHz).

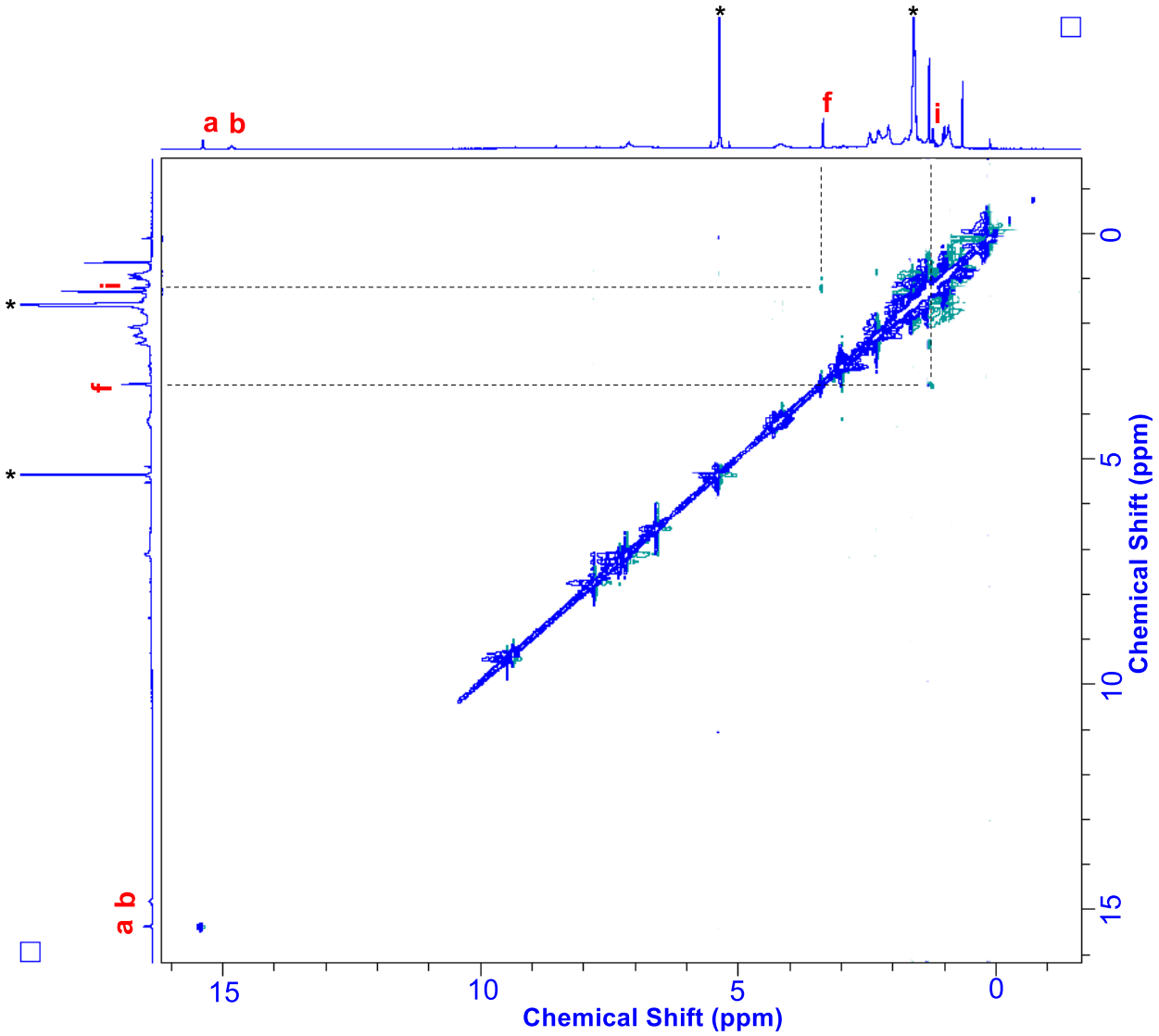

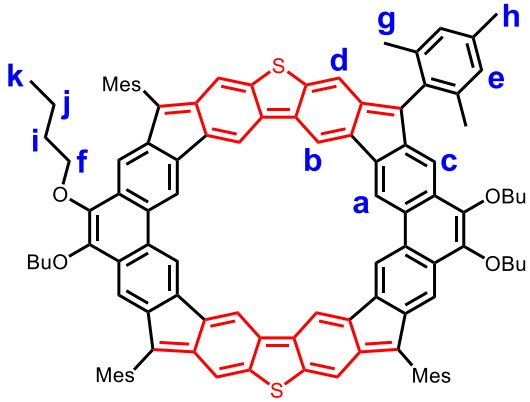

MC4-S

Figure S14. 2D ROESY NMR spectrum of **MC4-S** in CD_2Cl_2 at 298 K (500 MHz).

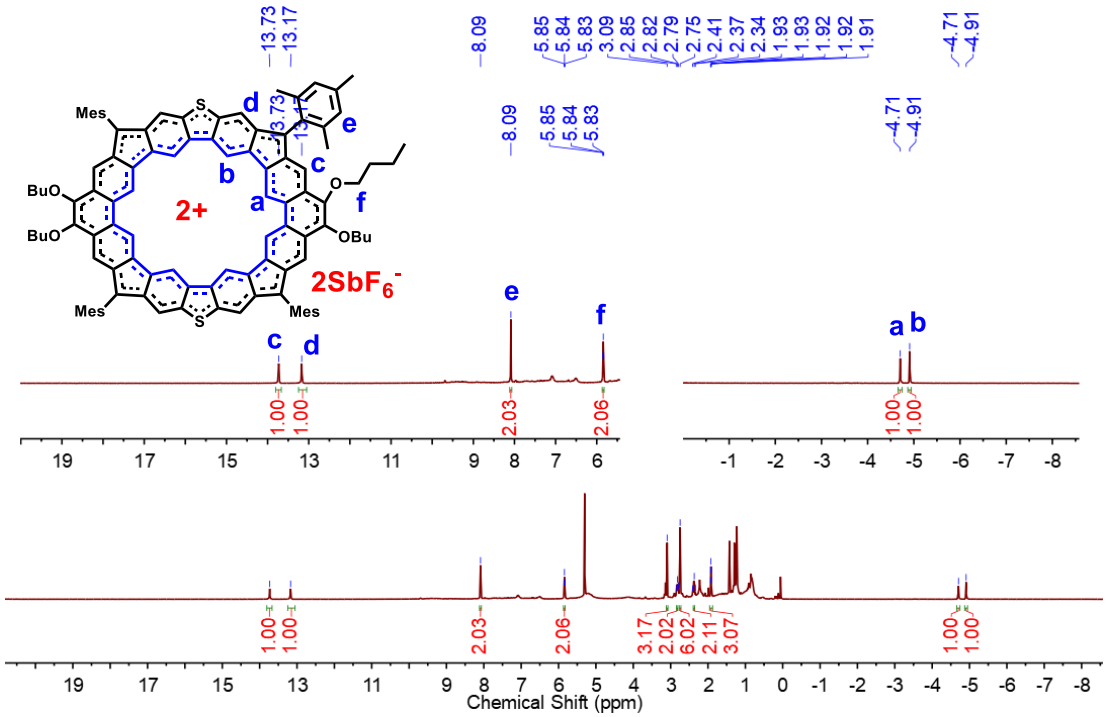

Figure S15. ^{1}H NMR spectrum of dication **MC4-S^{2+}** in CD_2Cl_2 at 298 K (125 MHz).

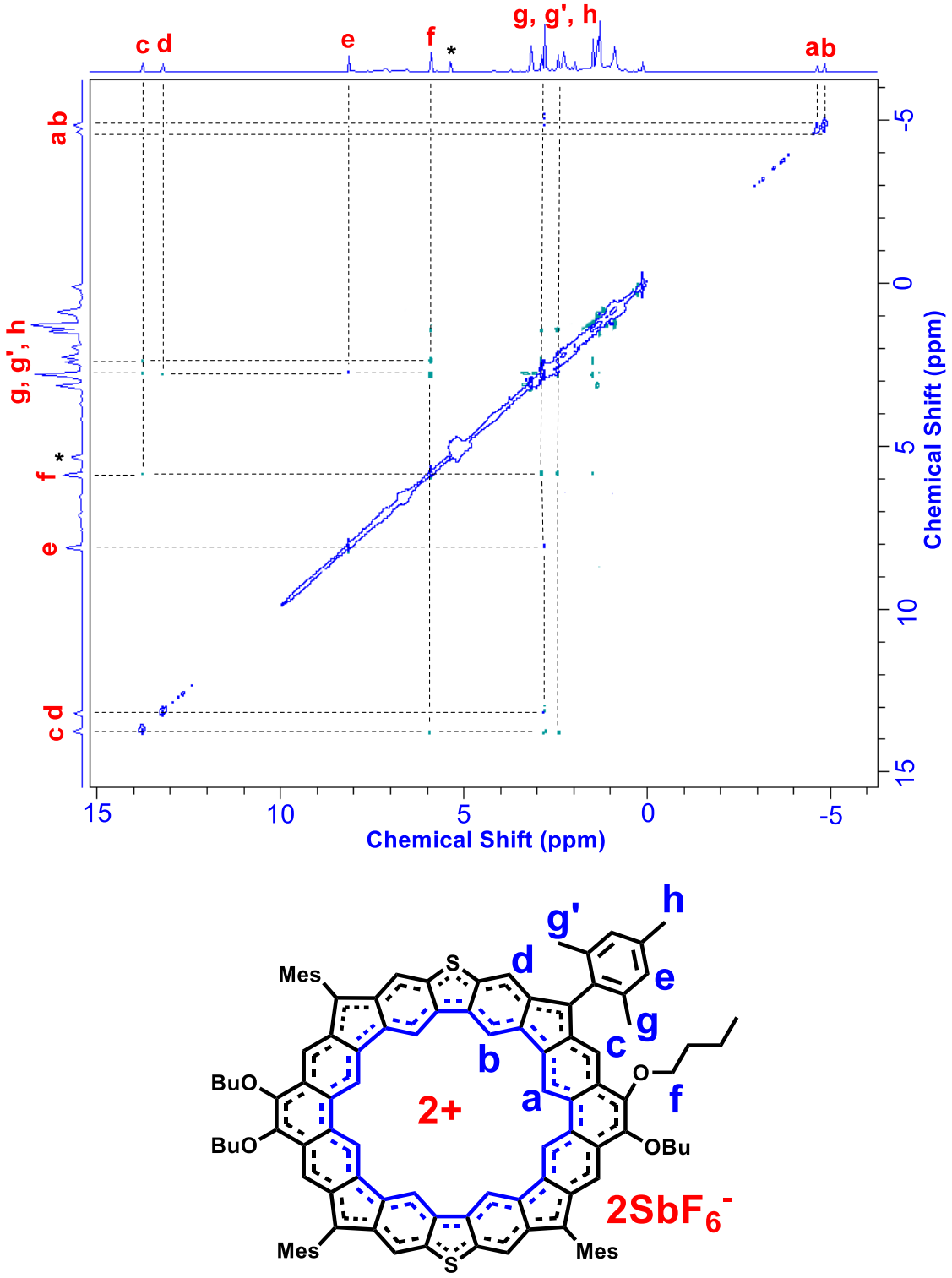

Figure S16. 2D NOESY NMR spectrum of dication **MC4-S**$^{2+}$ in CD_2Cl_2 at 298 K (500 MHz).

Mass Spectrum SmartFormula Report

Analysis Info

Analysis Name	D:\Data\Chem\2018 Samples\201808\0810\MC-Th-4CHO.d	Acquisition Date	8/10/2018 11:15:25 AM
Method	YCH-500-2500.m	Operator	default user
Sample Name	MC-Th-4CHO	Instrument / Ser#	micrOTOF-Q II 10269
Comment	Prof Wu Jishan		

Acquisition Parameter

Source Type	APCI	Ion Polarity	Positive	Set Nebulizer	3.0 Bar
Focus	Not active	Set Capillary	4500 V	Set Dry Heater	200 °C
Scan Begin	50 m/z	Set End Plate Offset	-500 V	Set Dry Gas	4.0 l/min
Scan End	2500 m/z	Set Collision Cell RF	800.0 Vpp	Set Divert Valve	Waste

Meas. m/z	#	Formula	m/z	err [ppm]	rdb	e⁻ Conf	N-Rule
1117.3791	1	C 72 H 61 O 8 S 2	1117.3802	1.0	42.5	even	ok

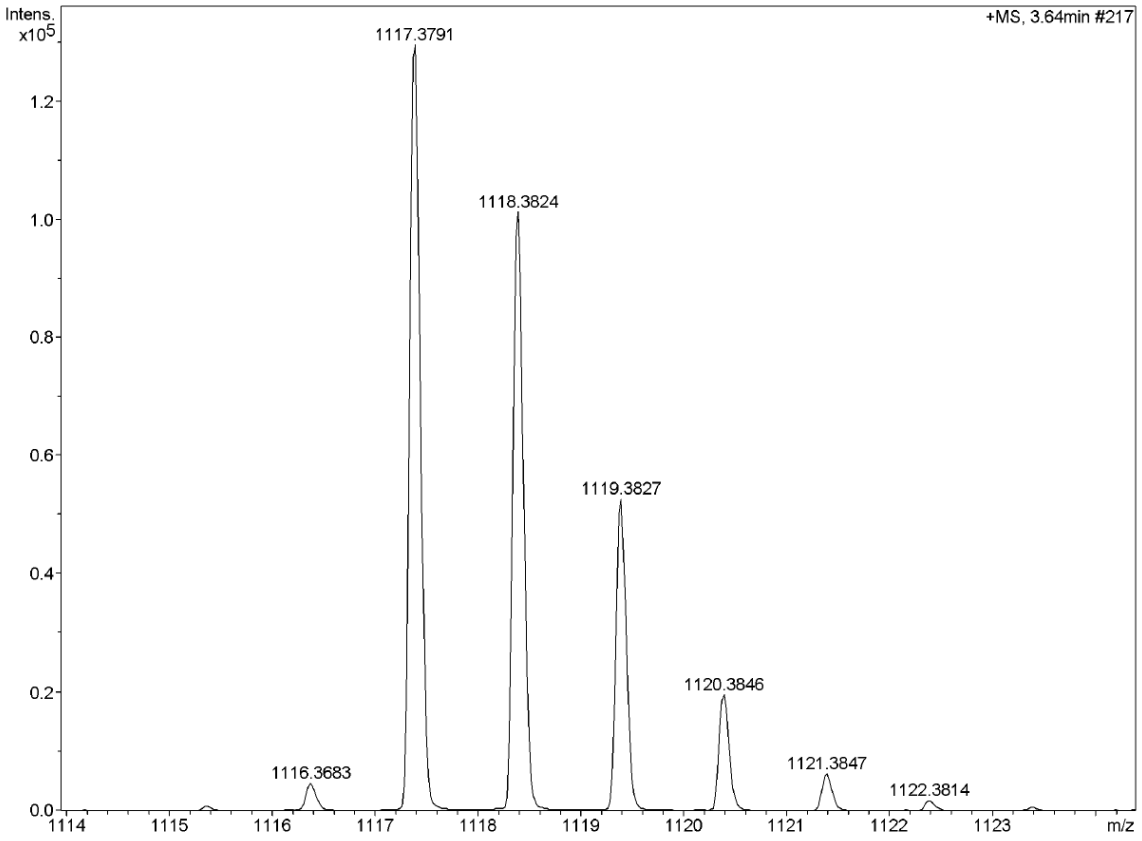

Figure S17. HR mass spectrum (APCI) of **3**.

Mass Spectrum SmartFormula Report

Analysis Info

Analysis Name	D:\Data\Chem\2018 Samples\201808\0810\MC-Th-4R.d	Acquisition Date	8/10/2018 12:11:39 PM
Method	YCH-500-2500.m	Operator	default user
Sample Name	MC-Th-4R	Instrument / Ser#	micrOTOF-Q II 10269
Comment	Prof Wu Jishan		

Acquisition Parameter

Source Type	APCI	Ion Polarity	Positive	Set Nebulizer	3.0 Bar
Focus	Not active	Set Capillary	4500 V	Set Dry Heater	200 °C
Scan Begin	50 m/z	Set End Plate Offset	-500 V	Set Dry Gas	4.0 l/min
Scan End	2500 m/z	Set Collision Cell RF	800.0 Vpp	Set Divert Valve	Waste

Meas. m/z	#	Formula	m/z	err [ppm]	rdb	e¯ Conf	N-Rule
1521.6820	1	C 108 H 97 O 4 S 2	1521.6823	0.2	60.5	even	ok

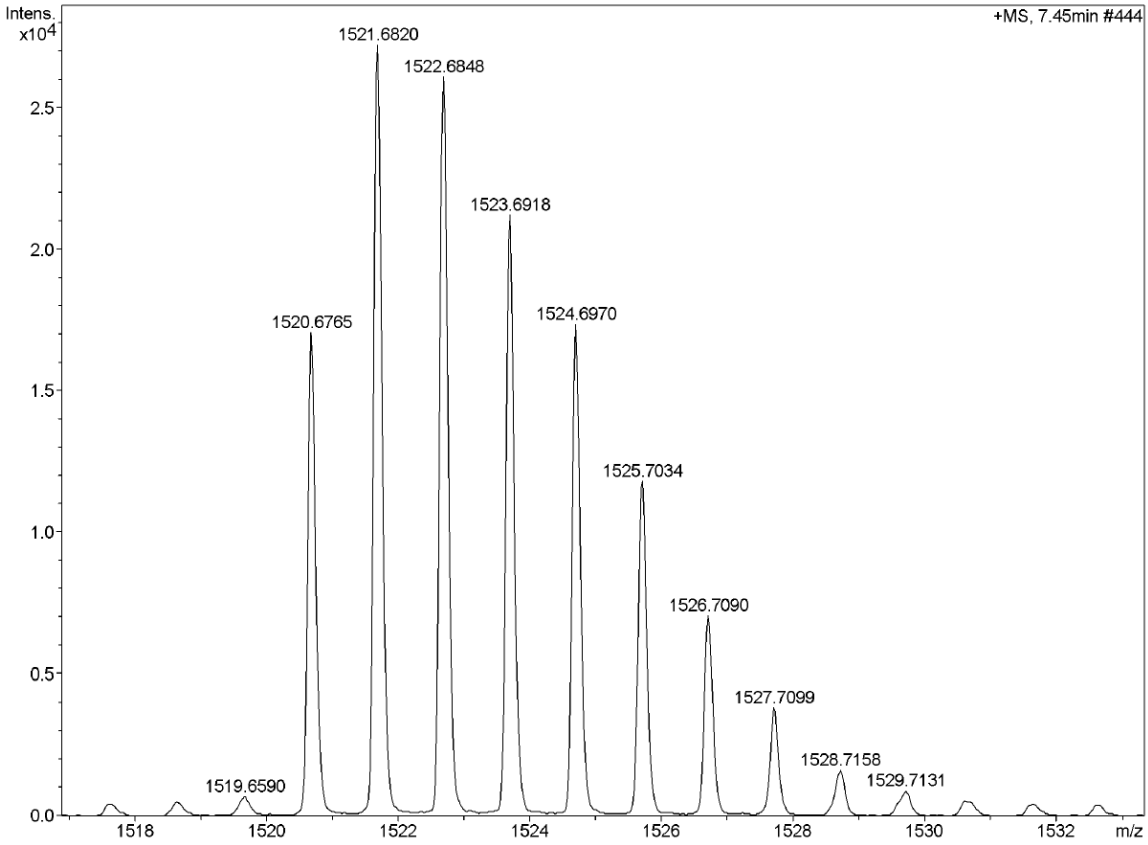

Figure S18. HR mass spectrum (APCI) of **MC4-S**.

6. References

1. M. A. Majewski, Y. Hong, T. Lis, J. Gregoliński, P. J. Chmielewski, J. Cybińska, D. Kim, M. Stępień, *Angew. Chem. Int. Ed.* **2016**, *55*, 14072

2. S. M. Kim, J. H. Kim, S. K. Jeon, J. Y. Lee, *Dyes and Pigments*, **2016**,125, 274.

3. Frisch, M. J.; Trucks, G. W.; Schlegel, H. B.; Scuseria, G. E.; Robb, M. A.; Cheeseman, J. R.; Scalmani, G.; Barone, V.; Mennucci, B.; Petersson, G. A.; Nakatsuji, H.; Caricato, M.; Li, X.; Hratchian, H. P.; Izmaylov, A. F.; Bloino, J.; Zheng, G.; Sonnenberg, J. L.; Hada, M.; Ehara, M.; Toyota, K.; Fukuda, R.; Hasegawa, J.; Ishida, M.; Nakajima, T.; Honda, Y.; Kitao, O.; Nakai, H.; Vreven, T.; Montgomery Jr., J. A.; Peralta, J. E.; Ogliaro, F.; Bearpark, M. J.; Heyd, J.; Brothers, E. N.; Kudin, K. N.; Staroverov, V. N.; Kobayashi, R.; Normand, J.; Raghavachari, K.; Rendell, A. P.; Burant, J. C.; Iyengar, S. S.; Tomasi, J.; Cossi, M.; Rega, N.; Millam, N. J.; Klene, M.; Knox, J. E.; Cross, J. B.; Bakken, V.; Adamo, C.; Jaramillo, J.; Gomperts, R.; Stratmann, R. E.; Yazyev, O.; Austin, A. J.; Cammi, R.; Pomelli, C.; Ochterski, J. W.; Martin, R. L.; Morokuma, K.; Zakrzewski, V. G.; Voth, G. A.; Salvador, P.; Dannenberg, J. J.; Dapprich, S.; Daniels, A. D.; Farkas, Ö.; Foresman, J. B.; Ortiz, J. V.; Cioslowski J.; Fox, D. J. *Gaussian 09*, Gaussian, Inc., Wallingford, CT, USA, **2009**.

4. (a) A. D. Becke, *J. Chem. Phys.* **1993**, *98*, 5648. (b) C. Lee, W. Yang, R. G. Parr, *Phys. Rev. B: Condens. Matter* **1988**, *37*, 785. (c) T. Yanai, D. Tew, N. Handy, *Chem. Phys. Lett.* **2004**, *393*, 51. (d) R. Ditchfield, W. J. Hehre, J. A. Pople, *J. Chem. Phys.* **1971**, *54*, 724. (e) W. J. Hehre, R. Ditchfield, J. A. Pople, *J. Chem. Phys.* **1972**, *56*, 2257. (f) P. C. Hariharan, J. A. Pople, *Theor. Chim. Acta* **1973**, *28*, 213.

5. D. Casanova, M. Head-Gordon, *Phys. Chem. Chem. Phys.* **2009**, *11*, 9779.

6. (a) Z. Chen, C. S. Wannere, C. Corminboeuf, R. Puchta, P. v. R. Schleyer, *Chem. Rev.* **2015**, *105*, 3842. (b) H. Fallah-Bagher-Shaidaei, S. S. Wannere, C. Corminboeuf, R., Puchta, P. V. R. Schleyer, *Org. Lett.* **2006**, *8*, 863.

7. D. Geuenich, K. Hess, F. Köhler, R. Herges, *Chem. Rev.* **2005**, *105*, 3758.

8. (a) S. Klod, E. Kleinpeter, *J. Chem. Soc., Perkin Trans. 2* **2001**, 1893. (b) T. Lu, F. Chen, *J. Comput. Chem.* **2012**, *33*, 580.

9. Saint Program included in the package software: **APEX3 v2016.1.0**

10. SADABS. Ver. 2014/5. Krause, L., Herbs-Irmer, R., Sheldrick, G. M. Stalke, D. (2015). *J. Appl. Crystallogr. 48.*

11. SHELXT-Integrated space-group and crystal-structure determination Sheldrick, G. M. *Acta Crystallogr., Sect. A* **2015**, A71, 3.

12. SHELXTL Sheldrick, G. M. Ver. 2014/7. Acta Crystallographica. *Sect C Structural Chemistry* 71, 3.

13. WinGX Farrugia, L. J. *J. Appl. Cryst.* **1999**, *32*, 837.